Are Heme Dependent Enzymes Always Using a Redox Mechanism? A Theoretical Study of the Kemp Elimination Catalysed by a Promiscuous Aldoxime Dehydratase.

Sergio Martí,[1] Iñaki Tuñón,[2,*] Vicent Moliner,[1,*] Joan Bertran[3]

1. Departament de Química Física i Analítica; Universitat Jaume I, 12071 Castellón (Spain)
2. Departament de Química Física, Universitat de València, 46100 Burjassot, (Spain)
3. Departament de Química; Universitat Autònoma de Barcelona, 08193 Bellaterra, (Spain)

Corresponding authors

I. Tuñón: tunon@uv.es

V. Moliner: moliner@uji.es

Abstract

The design of biocatalysts is a goal to improve the rate, selectivity and environmental friendship of chemical processes in biotechnology. In this regard, the use of computational techniques has provided valuable assistance in the design of enzymes with remarkable catalytic activity. In this paper, hybrid QM/MM simulations have allowed getting an insight into the mechanism of a promiscuous aldoxime dehydratase (OxdA) for the Kemp elimination. We first demonstrate that, based on the use of linear response approximation (LRA) methods, the lowest energy electronic state of the benzisoxazole placed in the active sit of OxdA corresponds to a singlet state, being the triplet and the quintet state higher in energy. The presence of a heme group in the active site of the OxdA promiscuous enzyme opens the possibility of exploring a redox mechanism, similar to the one proposed in other reactions catalysed by heme-dependent enzymes. In addition, according to the geometrical analysis of the active site of this aldoxime dehydratase, the presence of a good base in the active site, His320, the proper pose of the substrate assisted by the porphyrin and an adequate electrostatic environment to stabilize the negative charge developed in the oxygen leaving group, makes available an acid/base mechanism. Comparison of the results derived from the exploration of both acid/base and redox mechanisms at B3LYP(Def2-TZVP)/MM level, shows how the later render the most favourable reaction path within the quintet state. The obtained activation free energy is in good agreement with the activation energy that can be deduced from the experimentally measured rate constant.

Keywords: QM/MM, LRA method, Free Energies, Kemp elimination, aldoxime dehydratase, Heme containing enzymes, promiscuous enzymes.

1. Introduction

The Kemp elimination,[1] a reaction consisting in the decomposition of benzisoxazole to generate 2-cyanophenols (see Figure 1a),[2] has been the most popular benchmark for the design of new biocatalysts during the last years. The reaction, as shown in Figure 1, implies an asynchronous concerted proton transfer from a carbon atom to a heteroatom followed by the heterolytic N-O breaking bond and the formation of a nitrile group. Interestingly, there is no known natural enzyme whose primary reaction is the Kemp elimination, despite it has been demonstrated that there are many different systems that accelerate the reaction with different degree of efficiency.[3,4] Moreover, the synthesis of benzisoxazoles is quite straightforward from salicylaldehydes and the kinetic experiments are relatively easy to carry out due to the facility to detect the product with common spectroscopic techniques.[3]

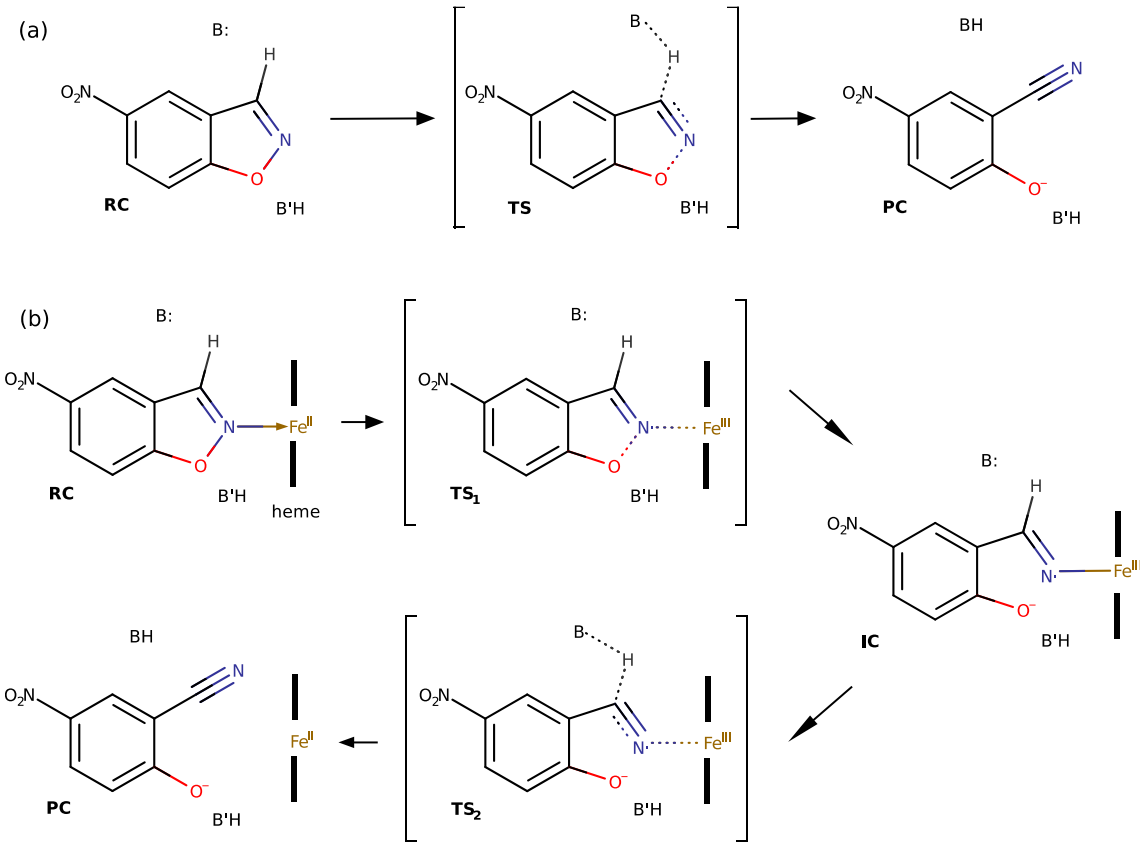

Figure 1. Two different mechanisms of the Kemp eliminases: (a) acid/base mechanism and (b) redox-mechanism.

The starting scaffolds employed in the protocol of the first *de novo* Kemp eliminase designs were based on different non-immunoglobulin proteins selected by means of Rosetta software employing a previously designed theozyme (a computational active site model) obtained by means of quantum mechanical calculations.[1] Based on the features of the optimized gas phase transition state (TS), two active-site motifs were considered as crucial in the new protein: a catalytic base for benzisoxazole

deprotonation and a hydrogen-bond donor to stabilize the developing negative charge on the phenolic oxygen atom (see Figure 1a). From a pull of experimentally characterized designs, each containing 10 to 15 mutations, eight of them resulted to be active. The X-ray diffraction analysis of one of the newly produced enzymes, was solved and demonstrated to superimpose well with the computational model. The activity was significantly improved by directed evolution and some of them, KE07,[5] KE70[6] and KE59,[7] were later used as templates for further rounds of mutations, optimizations and directed evolution, rendering more evolved and efficient Kemp eliminases.

A different approach for the development of new Kemp eliminases was applied by Mayo and co-workers based on a combination of X-ray crystallography and MD simulations on failed designs of new enzymes.[8] In particular, they used an iterative approach starting from an inactive protein scaffold, HG-1, that was designed to convert the xylan binding pocket of a thermostable xylanase into a Kemp eliminase. They found that the inactivity could be due to the lack of an optimized binding pocket. These findings guided the design of an active site deeply buried into the protein and, together with an additional mutation, the modified protein exhibited activity comparable to the best Rosetta design. Subsequent direct evolution produced a variant obtained in the Hilvert laboratory after 17 rounds of mutagenesis and screening (HG3.17).[9] This designed enzyme presents an exceptional efficiency, similar to highly optimized natural enzymes such as triosephosphate isomerase.[9]

Multiscale quantum mechanics/molecular mechanics (QM/MM) molecular dynamics (MD) simulations for the Kemp elimination in the HG3.17 enzyme demonstrated the presence of different conformations with significant different reactivity.[10] The larger reactivity was related with a better electrostatic preorganization of the environment that creates a more favourable electrostatic potential on the key atoms involved in the reaction; the oxygen atom of the aspartate acting as the base and the oxygen leaving group. Further analysis was carried out with similar computational methodologies on the less evolved HG3 confirming that its limitations can be related to a lack of flexibility, a not well fitted active site and a lack of protein electrostatic preorganization around the oxyanion hole.[11] Head-Gordon and co-workers confirmed the importance of the electrostatic preorganization in the efficient designs of previous Kemp eliminases and suggested that efficient computationally designed enzymes can be achieved with minimal experimental intervention using electric field optimization as guidance.[12,13,14] In contrast, despite the progress in this field during the last decade, it has been pointed out that the relevant advances in enzyme design are basically due to directed evolution with minor contributions from computational modelling.[15,16]

A different approach to design a Kemp eliminase can be based on the redesign of enzymes showing certain promiscuous activity for this reaction. These strategies are based on the introduction of mutations to increase this secondary activity through directed evolution or rational design. In

particular, attention has been put on two different kind of promiscuous enzymes; one of them would catalyse the reaction via the traditional acid/base mechanism (Figure 1a), while the second one would catalyse the reaction through a redox mechanism assisted by an active site heme group (Figure 1b).[17] A successful example of the redesign of the first group of promiscuous enzymes was achieved with Ketosteroid Isomerase (KSI), where mutations of residues acting as general base improved the catalytic efficiency for the Kemp elimination up to 7000 fold better than the wild-type.[18] An example of the second group of promiscuous enzymes is the P450-BM3 mutant, which was proven to be very active as a Kemp eliminase with a 10^7 fold larger rate constant over the uncatalyzed process in solution.[19,20] A combined theoretical-experimental study on this last enzyme shows that the reaction proceeds by an electron transfer from ferrous heme group to the substrate that provokes the N-O bond breaking (Figure 1b). Then, an internal rotation of the substrate has to take place to facilitate an intramolecular proton abstraction. The computational results indicate that this rotation is the rate limiting step.[19] When comparing catalytic activities of different Kemp eliminases, it must be kept in mind that some of them appear to catalyze the reaction through an acid-base mechanism while others, containing a Heme group, clearly use a redox pathway. Anyhow, the efficiency of the enzyme can be estimated by its rate constant, independently of the mechanism.

Other heme-contaning proteins have shown to catalyse the Kemp elimination, such as several aldoxime dehydratases (Oxd).[21] According to computational studies on one of them (OxdA), the primary reaction, consisting on the dehydration of aliphatic aldoximes (R−CH=N−OH) to the corresponding nitriles (R−C≡N), requires the participation of a histidine residue, His320. This residue would provide the proton to the aldoxime hydroxyl group during the first step, thus breaking the N-O bond. This is followed by the abstraction of the proton to form the final nitrile product. For this second step of the reaction, a rotation is required in the intermediate to properly orient the substrate towards His320, now acting as a base. It has been also postulated that the ferrous heme group, and not the ferric heme, is the one that is coordinated to the substrate aldoxime and catalyses the process, providing an electron to the substrate during the first step and receiving it back in the second one.[22,23] An interesting question is whether the secondary Kemp eliminase reaction catalysed by OxdA follows the same mechanism that the primary reaction, as previously assumed.[21] The purpose of the present study is to shed light into the mechanism employed by OxdA at atomic level, using QM/MM simulations. Moreover, considering that the heme group is involved in the catalysis of many processes, the knowledge of its role in the present reaction can have dramatic implications for the design of other heme-containing enzymes, a very active field in the scientific community. Despite it has been always assumed that heme

containing enzymes catalyse reaction through redox mechanisms, this has to be verified by electronic structure analysis, as demonstrated in this work.

2. Computational Methods

2.1. System set up. The initial geometry of the dimeric OxdA was obtained from the X-ray structure PDB id 3W08.[24] The pK_a of the tritratable amino-acids was calculated using the PropKa-3.1 program,[25,26] which predicted standard protonation states at pH 7. Histidine protonation states (delta/epsilon) were assigned by visual inspection, respecting the presence of hydrogen bonds with the surrounding residues, as determined form the X-ray structure. All hydrogen atoms were added using the psfgen tool provided with Namd-2.13[27] with the Charmm36[28,29,30] force field and the sidechains of the protein were subsequently optimized. At this point, we made use of Autodock Vina[31] for generating a total of 14 poses of the Kemp substrate in one of the active sites, in presence of the heme group. After inspection of the poses, we selected the one with the larger affinity energy. The model was then minimized keeping the backbone frozen, by means of conjugate gradient steps until convergence (gradient tolerance below 0.1 kJ/mol·Å). Thereupon, a total of 35 sodium cations (Na^+) were placed around the protein at optimal electrostatic positions in order to fulfill electroneutrality. The resulting system was then placed in an orthorhombic box of TIP3P water molecules of 120 x 100 x 80 $Å^3$ of size (a total of 698 and 27298 crystal and solvation water molecules, respectively). The solvated model was then fully optimized using the FIRE[32,33] algorithm (gradient tolerance below 10 kJ/mol·Å). We then performed 100 ns of molecular dynamics (MD) in the NVT ensemble at 300 K using a time step of 1 fs. The non-bonded interactions were treated using the Particle Mesh Ewald[34] method, with a cutoff of 16 Å and a maximum grid spacing of 0.5 Å. Once equilibrated, we used the resulting model to carry out the QM/MM potential energy surface (PES) exploration and free energy calculations. For this purpose, we defined a subset of QM atoms comprising: the substrate, part of the heme group (without the side chains), the axial His299 ligand of the iron atom, the Hiss320 acting as a base, the Ser219 and a crystal water molecule (see Figure 2). These two last residues are not directly involved in the reaction mechanism, but due to their proximity to the substrate they are likely to stabilize the formation of the oxy-anion by means of charge transfer effects. A total of 11 hydrogen link-atoms were needed, in addition to the 75 selected QM atoms, to fulfil their valences. From this point and hereupon, all the calculations on the system were performed keeping fixed any molecule or residue found more than 20 Å apart of the QM atoms. The MM atoms were described using Namd with the Charmm36 force-field, while for the QM ones we used the B3LYP[35,36] density functional method combined with the Lanl2DZ[37] basis set, as implemented in the Gaussian09[38] package of programs. To obtain more reliable results, single point energy calculations were performed on the optimized

structures using the same functional but using an all-electrons polarized triple zeta basis set, Def2-TZVP,[39] for all the atoms. Dispersion corrections were added using the Grimme DFT-D3(BJ).[40,41] Analysis of the electronic density of all involved stationary structures has been carried out the Natural Bonding Orbital, NBO approach,[42] as implemented in Gaussian 09.

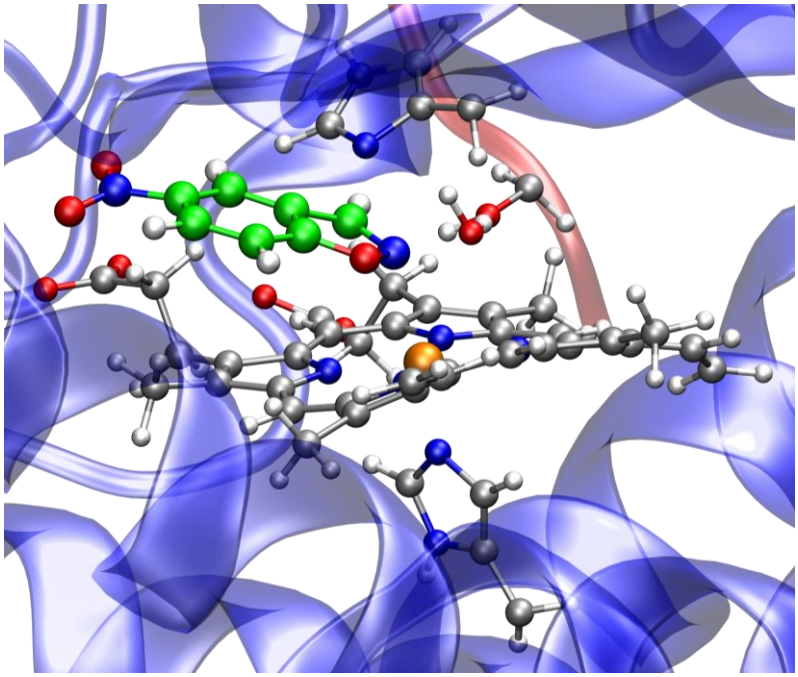

Figure 2. Detail of the active site of the OxdA. QM subset of atoms are displayed as ball and sticks: the carbon atoms of the substrate in green and of the heme group and key residues His320, Ser219 in grey.

2.2. Exploration of the Reaction Mechanisms. The reaction mechanism was initially explored in three different spin states of the heme iron atom: singlet, triplet and quintet, depending on the kind of crystal field and the spin distribution (low- or high-spin). Each step of the proposed mechanisms was studied initially performing the localization of the corresponding transition structure (TS), using a micro/macro optimization scheme.[43] Once characterized and verified the nature of each TS (presenting one and only one imaginary frequency associated to the chemical step under inspection), the reaction paths were traced towards the intermediate, reactant or product species. The end points of each path were afterwards optimized and characterized as stationary points corresponding to a minimum. The coordinates of the stationary structures are given in Table S1 of the Supporting Information.

2.3. Relative Stability of Spin States. In order to evaluate the relative stability among the different spin states of the reactants we estimated the free energy difference among them, because potential energy differences can be highly dependent on the nature of the local minima used to evaluate it. For this

purpose, we used the linear response approximation (LRA),[44,45] which offers a perturbative estimate of the relative free energy. In principle, the free energy difference could be evaluated from simulations carried out in the initial and final states:

$$\Delta F_{i\to j} \approx \frac{1}{2}\left(\langle U_j\rangle_i - \langle U_i\rangle_i - \langle U_i\rangle_j + \langle U_j\rangle_j\right) \quad (1)$$

where $\Delta F_{i\to j}$ is the variation of free energy needed to change from the state i to j, U_x are the corresponding potential energies of the given states, and the $\langle \quad \rangle_x$ denotes that the averages are carried out for this state. Thus, series of QM/MM MD on the reactant species at the three different electronic states (singlet, triplet and quintet) were performed, and then the change in potential energy associated with the spin swapping was evaluated. A total of 10 ps of NVT MD for each species was needed, to achieve convergence of eq 1, as demonstrated by the calculated standard deviations. Details about the LRA calculations and error estimations are provided in the Supporting Information.

3. Results

3.1. Analysis of Reactant States. As mentioned in the Introduction section, despite iron can initially present two oxidation states, Fe(III) and Fe(II), in the heme group, it has been experimentally proved that the later shows rate constants for this reaction two-folds higher than the former.[21] Consequently, our study was focused in exploring the reactivity of OxdA with the heme group starting from Fe(II) in the three possible multiplicity states: singlet, triplet and quintet. Then, the first step in our study was to establish the relative energies of the different electronic states of reactants. Keeping in mind the size and flexibility of our system, this evaluation should not be based on just a comparison of potential energies of a single structure for each of the three different electronic configurations. Instead, a proper comparison must take into account an average performed on the configurations sampled by the system, since small conformational changes of the environment, unrelated to the chemical steps, can disguise the relative energy distribution of the compared species. For this reason, as described in the Methods section, relative free energies between the three possible electronic states at the reactants were computed using the linear response approximation.

The results of our QM/MM simulations performed with the Lanl2DZ basis set show how the most stable reactants state corresponds to the singlet state, being the quintet and triplet states located at 3.8 ± 0.6, and 14.3 ± 0.6 kcal·mol^{-1}, respectively, above the singlet one. Since the triplet state was found at a significantly higher energy, only the singlet and quintet states were considered to perform single point energy calculations with the larger Def2-TZVP basis set. The results for this basis set show that the singlet is still the most stable, being the quintet state now located at 2.8 ± 0.6 kcal·mol^{-1} above (see Supporting Information for details). In a computational study by Liao and Thiel in a heme-dependent

aldoxime dehydratase (OxdRe), the same trend of the three electronic states in the primary reaction was found, despite the evaluation of the relative ordering was based on single molecule energy optimizations.[23] However, this trend is not in agreement with the relative values reported by Li, Wang and co-workers for the Kemp eliminase reaction catalysed by P450-BM3 who, based on QM/MM potential energy calculations, reported the singlet state as the one with the highest energy and the quintet state 2.0 kcal·mol^{-1} more stable than the triplet state.[19] As commented before, our estimations based on statistical simulations are more reliable. It is interesting to note that during our simulations we found instantaneous configurations where the stability ordering of the different electronic states differs from that obtained from the average result (see Figure S1 of Supporting Information), demonstrating the necessity of an adequate sampling procedure to properly establish which is the most stable electronic configuration.

A detail of the average structure of the active site obtained along the QM/MM MD simulation of the singlet state is shown in Figure 3, where the values of key distances of the three states are reported.

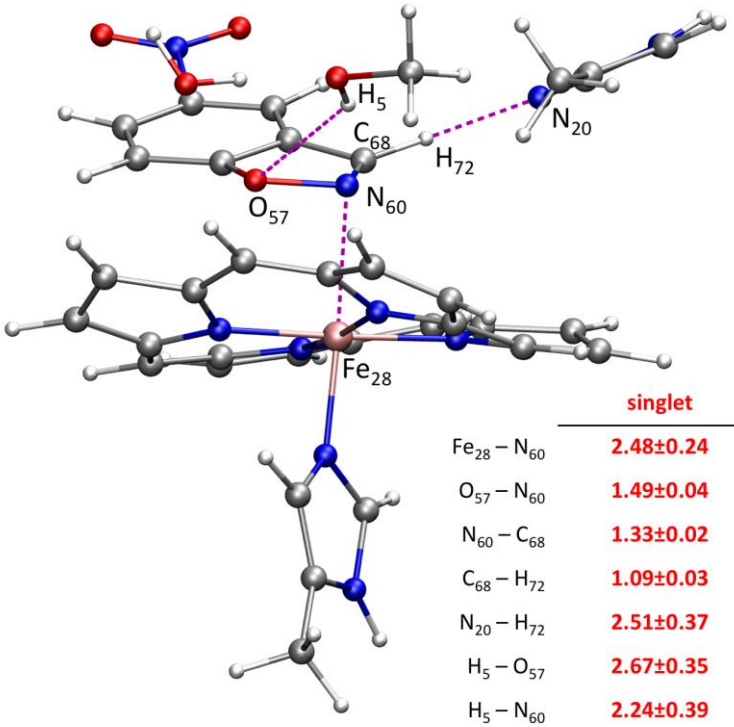

	singlet	triplet	quintet
$Fe_{28} - N_{60}$	2.48±0.24	2.93±0.14	3.24±0.42
$O_{57} - N_{60}$	1.49±0.04	1.49±0.04	1.50±0.04
$N_{60} - C_{68}$	1.33±0.02	1.33±0.02	1.33±0.02
$C_{68} - H_{72}$	1.09±0.03	1.10±0.03	1.10±0.03
$N_{20} - H_{72}$	2.51±0.37	2.48±0.36	2.31±0.26
$H_5 - O_{57}$	2.67±0.35	2.87±0.68	3.57±0.47
$H_5 - N_{60}$	2.24±0.39	2.31±0.66	3.15±0.58
$C_{68} - H_{72} - N_{20}$	154.8±11.7	165.6±7.5	163.4±7.6

Figure 3. Snapshot of the average structure of the active site obtained along the QM/MM MD simulations of the singlet state. Key average distances (in Å) and angles (in degrees) obtained with the are reported for the singlet, triplet and quintet states.

As can be deduced from the analysis of Figure 3, despite the structures are quite close to each other, some differences can be highlighted. Thus, the average distance between the N_{60} and Fe atoms ranges

between 2.48 Å in singlet state to 2.93 and 3.24 Å in triplet and quintet states, respectively. The slightly shorter distance in the singlet state is nevertheless not correlated to an elongation of the other two covalent bonds involving N_{60} (N_{60}-O_{57} and N_{60}-C_{68}), as deduced from the comparison with the triplet and quintet state averaged structures. The approximation of the substrate to the Fe atom in the singlet state is not correlated neither to any relative movements between the porphyrin and Ser219 or His320. In all, no dramatic geometric differences are detected by comparing the reactant state in its three different electronic states.

3.2 Reaction Mechanisms. Kemp eliminase reaction implies the proton transfer from benzisoxazole to a base (His320) and an electron transfer to the antibonding orbital of the N_{60}-O_{57} bond to break this bond and form a nitrile group. After a deep analysis of the QM/MM optimized geometries of the active site of the heme-dependent OxdA promiscuous enzyme, two alternative mechanisms can take place. These are a redox-mediated process, where the heme group acts as electron donating group (see Figure 1b) and the traditional acid/base mechanism (see Figure 1a) similar to that described in the HG-3 and HG3.17.[10,11] In the former, the reaction proceeds in a stepwise manner. First, an inter-molecular electron transfer takes place from the Fe atom of the heme group to the antibonding orbital of the N_{60}-O_{57} bond of the substrate with the concomitant ring opening (see Figure 1b). In the second step, the proton is transferred from the substrate to His320 and an electron is transferred back to the Fe atom from the substrate. In the second feasible Kemp eliminase mechanism (Figure 1a), a base in the active site (His320) is capable of abstracting a proton from the substrate concomitant with the breaking of the N_{60}-O_{57} bond and formation of the N_{60}-C_{68} triple bond. The abstraction of the proton from the C_{68}-H_{72} bond provokes an intramolecular electron transfer to the antibonding orbital of the N_{60}-O_{57} bond of the substrate. It is important to point out that studies of the Kemp eliminase reaction catalysed by other heme-dependent enzymes such as P450-BM3 by Shaik, Reetz and co-workers has been exclusively described as a redox-mediated process.[19] In P450-BM3, the absence of a base in the active site makes the traditional acid/base mechanism unaffordable. The results derived from the exploration of the two alternative Kemp elimination mechanisms catalysed by OxdA in the singlet and quintet electronic state, computed at B3LYP/MM level, with the def2-TZVP basis set for all QM atoms, are described below. The results obtained with the Lanl2DZ basis set, and those for the triplet state are deposited in the Supporting Information.

3.2.1. Redox-mediated Mechanisms. The QM/MM free energy profiles for the redox Kemp elimination in the singlet and quintet states catalysed by the promiscuous OxdA enzyme are shown in the left side of Figure 4. Notice that in the quintet state two different electronic configurations can be found: one

with a ferromagnetic coupling between the Fe and N_{60} atoms (denoted as quintet-ferro), and the one with an antiferromagnetic coupling (quintet-antiferro). The reaction takes place in two steps on the potential energy surfaces in the three possible electronic states. When adding the thermal and zero-point energy corrections to get the free energy profiles, the second step becomes barrierless in the quintet-ferro state, almost barrierless in the quintet-antiferro state. Then, according to the free energy profiles, and considering the relative energies of the reactant states discussed above, the most favourable redox mechanism of the Kemp eliminase reaction catalyzed by the promiscuous OxdA enzyme would take place through the quintet-antiferro state. The overall activation free energy of 13.6 kcal·mol^{-1}, dictated by the first step, is in good agreement with the activation energy that can be deduced from the experimentally measured rate constants by Asano and co-workers at 23 ºC, of 16.0 kcal·mol^{-1}.[21] For this first step, the TS free energies of the singlet state relative to the singlet reactants state is 27.7 kcal·mol^{-1}, while those for the quintet-ferro and quintet-antiferro state are 35.3 and 13.6 kcal·mol^{-1}, respectively. The results suggest that the minimum energy path corresponds to the redox-process in the quintet-antiferro state. Considering that the most stable reactant state is in the singlet state, an intersystem crossing must occur between reactants and the first transition state, TS_1. From this point on, the reaction takes place without an electronic spin change. Otherwise, the quintet-antiferro reactants state can also present certain population at room temperature, since the free energy of this electronic state is just 2.8 kcal·mol^{-1} above the singlet reactant state. This would imply no spin transition along the full process. As can be deduced from the inter-atomic distances of the involved states listed in Table 1, the first step involves the shortening of the distance between the substrate and the heme group in order to favour the electron transfer (see distance Fe-N_{60} in Table 1). This approach is concomitant with the lengthening of the breaking bond of the substrate, N_{60}-O_{57}. In the second step, the proton from C_{68} atom of the substrate is transferred to His320. The negative charge developed in the phenolate oxygen atom, O_{57}, is partially stabilized by a hydrogen bond interaction with Ser219 (see O_{57}-H_5 distance in Table 1). Finally, the substrate departs from the heme group, being the final distance between Fe and N_{60} above 3 Å in the three electronic states.

In an attempt to explore the phenolic oxygen as an alternative base, instead of the His320, the intramolecular proton transfer between the atoms C_{68} and O_{57}, starting from the most stable intermediate compound, was explored. The potential energy surface obtained for the quintet-antiferro state shows an exothermic process with an potential energy barrier of 8.3 kcal·mol^{-1} from the intermediate (see Figure S2 of the Supporting Information). This result demonstrates that the almost barrierless intermolecular His320 mediated mechanism is the kinetically favoured process for the proton abstraction (see Figure 4).

The analysis of the spin density on the key atoms, N_{60} and Fe, reveals similar behaviour for all spin states in the redox mechanism (see Table 2). The electron density on the Fe is decreased by almost one electron from reactants to the intermediate, while it is increased by almost the same amount in the N_{60} atom. Part of the spin density is also found on O_{57} and C_{68} atoms. The values obtained from the intermediates and products confirms that the electron is transferred back to the Fe in the second step. The participation of the substituents of the Fe, the porphyrin and the axial His229, in the electron transfer process is minor.

A deeper insight into the electronic orbital evolution along the reaction path based on the second order perturbation theory analysis (see Supporting Information, Table S4), shows that during the first step of this redox mechanism, there is a significant donation from the Fe atom to the N_{60}-O_{57} antibonding orbital and also, to a minor extent, from the occupied N_{60}-O_{57} bonding orbital to a vacant orbital of the Fe atom. In this second step, a significant delocalization between the N_{60} lone pair and the antibonding C_{68}-H_{72} orbital is detected, thus contributing to the proton abstraction. We also observed delocalization between the occupied C_{68}-H_{72} bonding orbital and a vacant lone pair of the N_{60} atom and from a lone pair of N_{60} atom to a vacant orbital of the Fe atom. This suggests that, after proton abstraction, an electron is transferred back from C_{68}-H_{72} to N_{60}, and from N_{60} to the Fe atom of the heme group.

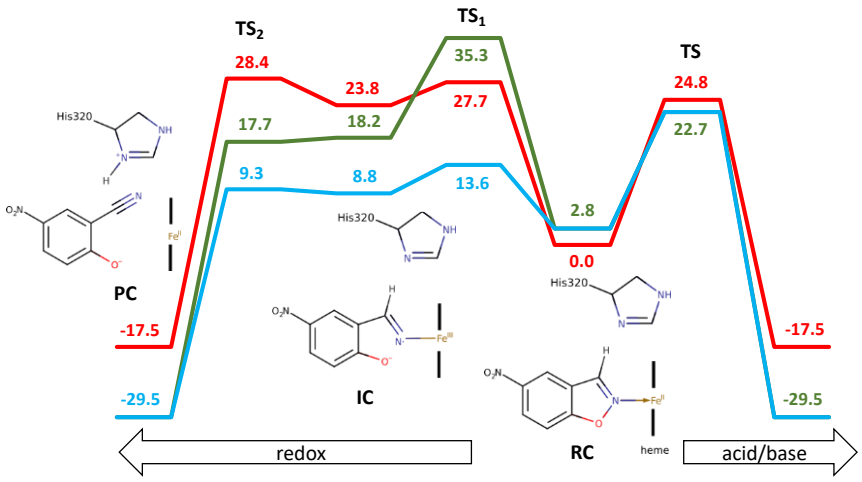

Figure 4. B3LYP(Def2-TZVP)/MM free energy profiles (in kcal·mol^{-1}) for the redox Kemp elimination catalysed by the promiscuous OxdA enzyme by means of two different mechanisms starting from the same reactant complex (RC): acid/base (from RC to the right) and redox (from RC to the left). Red line represents the reaction in the singlet electronic state, the green line is the reaction in the quintet state with ferromagnetic coupling between the Fe and N_{60} atoms, while the quintet state with an antiferromagnetic coupling is shown with the blue line.

Table 1. Relative free energies obtained with the Def2-TZVP basis set, ΔG (in kcal·mol^{-1}), and key interatomic distances (in Å), for the different states appearing along the reaction in the singlet and quintet states for the two located mechanisms: redox and acid/base.

			redox			acid/base	
	state	**RC**	**TS1**	**IC**	**TS2**	**TS**	**PC**
ΔG	singlet	0.0	27.7	23.8	28.4	24.8	-17.5
	quintet-F	2.8	35.3	18.2	17.7	22.7	-29.5
	quintet-A	2.8	13.6	8.8	9.3	22.7	-29.5
$Fe–N_{60}$	singlet	2.81	1.91	1.91	1.91	2.96	3.01
	quintet-F	3.16	2.35	2.27	2.12	3.34	3.47
	quintet-A	3.16	2.06	2.06	2.12	3.34	3.47
$O_{57}–N_{60}$	singlet	1.50	2.24	2.27	2.62	1.75	3.43
	quintet-F	1.49	2.21	2.50	2.53	1.70	3.69
	quintet-A	1.49	2.29	2.27	2.52	1.70	3.69
$N_{60}–C_{68}$	singlet	1.33	1.31	1.31	1.26	1.29	1.19
	quintet-F	1.33	1.30	1.31	1.26	1.30	1.18
	quintet-A	1.33	1.31	1.31	1.26	1.30	1.18
$C_{68}–H_{72}$	singlet	1.10	1.11	1.11	1.38	1.40	2.45
	quintet-F	1.10	1.11	1.11	1.32	1.54	2.59
	quintet-A	1.10	1.11	1.12	1.32	1.54	2.59
$N_{20}–H_{72}$	singlet	2.00	2.29	2.29	1.44	1.30	1.02
	quintet-F	2.02	2.09	2.14	1.49	1.24	1.03
	quintet-A	2.02	2.17	2.17	1.50	1.24	1.03
$O_{57}–H_5$	singlet	2.19	2.38	2.38	1.60	1.84	1.67
	quintet-F	3.59	2.47	2.65	1.58	3.53	1.64
	quintet-A	3.59	2.41	2.45	1.66	3.53	1.64
$N_{60}–H_5$	singlet	1.87	2.02	2.01	2.58	2.28	2.98
	quintet-F	3.46	1.90	1.91	2.52	3.65	3.37
	quintet-A	3.46	1.95	1.91	2.52	3.65	3.37

Table 2. Spin densities obtained with the Def2-TZVP basis set (in a.u.) for the different states appearing along the reaction in the singlet, triplet and quintet state for the two located mechanisms: redox and acid/base

			redox			acid/base	
	state	**RC**	**TS1**	**IC**	**TS2**	**TS**	**PC**
O_{57}	singlet	0.00	-0.20	-0.07	-0.03	0.00	0.00
	quintet-F	0.00	0.17	0.07	0.09	0.00	0.00
	quintet-A	0.00	-0.18	-0.06	-0.04	0.00	0.00
N_{60}	singlet	0.00	-0.47	-0.70	-0.40	0.00	0.00
	quintet-F	-0.01	0.75	0.86	0.79	0.00	0.00
	quintet-A	-0.01	-0.51	-0.64	-0.43	0.00	0.00
C_{68}	singlet	0.00	0.03	0.05	-0.02	0.00	0.00
	quintet-F	0.01	-0.04	-0.03	0.02	0.00	0.00
	quintet-A	0.01	0.08	0.09	0.05	0.00	0.00
H_{72}	singlet	0.00	-0.03	-0.05	-0.04	0.00	0.00
	quintet-F	0.00	0.05	0.06	0.07	0.00	0.00
	quintet-A	0.00	-0.04	-0.05	-0.05	0.00	0.00
Fe	singlet	0.00	0.77	0.92	0.68	0.00	0.00
	quintet-F	3.82	3.01	2.95	2.86	3.83	3.77
	quintet-A	3.82	4.19	4.22	4.14	0.00	0.00
Porphyr.	singlet	0.00	-0.06	-0.07	-0.07	0.00	0.00
	quintet-F	0.11	-0.06	-0.04	-0.10	0.11	0.17
	quintet-A	0.11	0.39	0.40	0.07	0.00	0.00
His229	singlet	0.00	-0.01	-0.02	-0.05	0.00	0.00
	quintet-F	0.00	0.01	0.02	0.06	0.00	0.00
	quintet-A	0.00	-0.01	-0.03	-0.04	0.00	0.00

3.2.2. Acid/base Mechanism. The presence of a properly located base in the active site of OxdA, a histidine residue (His320), suggests that the traditional acid/base mechanism could be also feasible in this enzyme. This is first confirmed by the analysis of the relative orientation of the substrate in the active site after equilibration of the reactant complex structures (see Figure 3 and Table 1), that shows how His320 is at hydrogen bond distance of the C_{68}-H_{72} bond. Our simulations indicate that the interaction between the substrate and the heme group contributes to facilitate the pose of the former in the active site along the full process. The exploration of this mechanism shows how the reaction can take place in the active site of OxdA through a single step acid/base mechanism, regardless of the electronic state. This mechanism is similar to the one previously characterized by other *de novo* Kemp eliminases such as HG-3 or HG-3.17,[10,11] where the base of the active site abstracting the proton was

an aspartate residue. As shown in the right side of Figure 4, and in Table 1, the free energy barriers of the acid/base mechanism measured from their corresponding reactants states were 24.8 and 22.7 kcal·mol^{-1} for the singlet and quintet states, respectively.

As deduced from Table 2 for this acid/base mechanism, the spin density on the Fe atom reveals to be invariant along the reaction in the three electronic states, in accordance with the absence of an inter-molecular electron transfer between the heme group and the substrate. Second order perturbation theory analysis (see Supporting Information) shows that, in this mechanism, electron transfer to the N_{60}-O_{57} antibonding orbital comes essentially from the C_{68}-H_{72} bonding orbital, being thus promoted by the concomitant proton transfer.

4. Discussion

The analysis of the results shows that OxdA offers two alternative mechanistic routes for the Kemp elimination reaction: redox and acid/base. As shown in Figure 4 and Table 1, the lowest free energy reactant state corresponds to the singlet electronic configuration. From this point on, the reaction catalysed by OxdA preferentially takes place using a step-wise redox mechanism through a quintet electronic state with an antiferromagnetic coupling between Fe and N_{60} atoms. The kinetics of the process is determined by the first step, with a free energy barrier of 13.6 kcal·mol^{-1} with respect to the most stable reactants. The most favourable reaction path through the alternative acid/base mechanism would also take place in the quintet state, but with a significantly higher free energy barrier; 22.7 kcal·mol^{-1}. Thus, only the redox mechanism offers a significant improvement of the kinetics by comparison to the uncatalyzed reaction in solution, that presents an experimentally derived free energy barrier of 23.4 kcal·mol^{-1}.[6]

The preference for the quintet state has been assessed based on free energy calculations that provide more robust conclusions about the relative ordering of the spin states than single structure potential energy calculations. An electronic density analysis of the averaged structures of the reactants states shows that the singlet state shows the highest value of the dative bond between the N_{60} atom of the substrate and the Fe atom of the heme group. The Wiberg index of Fe-N_{60} bond takes values of 0.26 and 0.06 at the reactants state of the singlet and quintet configurations, respectively. The formation of this partial bond is reflected in a smaller interatomic distance between Fe and N_{60} atom in the singlet state, as shown in Figure 3. This dative bond is also reflected in the charge of the Fe atom, that takes values of 0.23 and 0.90 a.u. in the singlet and quintet configurations, respectively. The second order perturbation analysis (see Table S4 of the Supporting Information) of the interaction between a vacant orbital of the Fe atom and the lone pair orbital of the N_{60} atom confirms a significant larger coupling between these orbitals in the singlet state. This picture confirms how the enzyme, and in particular the

heme group, interacts and stabilizes further the reactants state when the substrate is in the singlet electronic configuration, in agreement with the relative free energies of the reactants derived from our statistical simulations.

As discussed in the previous section, the Kemp eliminase reaction requires an electron transfer to the N_{60}-O_{57} antibonding orbital in order to cleave it. This transfer can be intermolecular, i.e. redox mechanism, or intramolecular, i.e. acid/base mechanism. In principle, the intramolecular electron transfer must be considered as more effective than the intermolecular process, although the former requires that the proton abstraction (H_{72}) precedes the electron transfer, in order to form a transient carbanion species from which the electron can be transferred. Instead, in the redox mechanism the proton abstraction takes place after the electron transfer. In both cases the proton abstraction requires of the presence of an adequate external base and of the electrostatic stabilization of the negative charge that is finally developed on the oxygen leaving group (O_{57}).[10,11] OxdA offers these two requirements. First the presence of a well-positioned base in the active site, His320 and, second, a positive electrostatic potential generated by the full enzyme on O_{57}; 173 ± 27 and 144 ± 18 $kJ \cdot mol^{-1} \cdot e^{-1}$ computed in the reactants state of the singlet and quintet electronic configurations. Interestingly, the stabilization that can be deduced from these positive electrostatic potentials on the negative charge developed on the oxygen leaving group correlate with the computed relative energies of the reactants states.

The characteristics of the OxdA enzyme are comparable to those found in other Kemp eliminases, such as the HG3.17 *de novo* design. In this enzyme the base in the active site is an aspartate, and a favourable positive electrostatic potential on the oxygen leaving group was generated by the full enzyme and water molecules present in the active site.[10,11] The active site water molecules in HG3.17 have roles with opposite effects; they contribute to the favourable electrostatic potential on the leaving group of the substrate but, on the other side, they also solvate the aspartate of the active site, thus diminishing its base character.[10] In OxdA, the base is a histidine residue, an intrinsically weaker base than aspartate, but the absence of water molecules in the surroundings of His320 could explain the ability of this enzyme to virtually transform the second step of the redox mechanism (the proton abstraction) into a barrierless process. Other heme dependent Kemp eliminases do not present a base correctly placed in the active site to abstract the hydrogen from the substrate. This impedes the proton abstraction and the subsequent intramolecular electron transfer and, thus, the only available reaction mechanism is the redox one where the electron transfer to the N_{60}-O_{57} antibonding orbital takes place from the heme group in a first step, and then an intramolecular proton transfer takes place in the substrate.

5. Conclusions

We herein present a theoretical study of the Kemp eliminase reaction catalysed by a promiscuous aldoxime dehydratase, OxdA. The reaction basically consists in the substrate proton abstraction by a base and the breaking of the N_{60}-O_{57} bond to form a nitrile group. First, we demonstrate that the lowest energy electronic state of the benzisoxazole-heme reactant complex placed in the active sit of OxdA corresponds to a singlet state, being the quintet state 2.8 kcal·mol^{-1} higher in free energy. The triplet state is located 14.3 kcal·mol^{-1} above the singlet one and, consequently, this electronic state was not considered in the study of the full reaction mechanism. It is important to stress that the evaluation of the relative stability among the three different spin states of the reactants were not obtained by evaluation of the potential energy differences of three single structures, a procedure that can be highly dependent on the nature of the localized minima. Instead, we employed average free energies as obtained from linear response approximation (LRA) methods. The origin of the singlet state stabilization appears to be related with the presence of a dative bond between the N_{60} atom of the substrate and the Fe atom of the Heme group. The full protein is thus stabilizing reactive conformations of the substrate in this electronic configuration as proved by analysis of electron densities and geometries.

The presence of a Heme group in the active site of the OxdA promiscuous enzyme opens the possibility of exploring a redox mechanism, similar to the one proposed in other reactions catalysed by heme-dependent enzymes. In the present study, our results indicate that the reaction catalysed by the heme containing OxdA takes place through a two-step redox process. In the first step, the heme group is the fragment that donates an electron to the antibonding orbital between the N_{60} and the O_{57} atom, thus facilitating the breaking of this bond. In the second step an electron transfer takes place from the N_{60} lone pair to the antibonding of the C_{68}-H_{72}, thus contributing to the proton transfer to the His320 residue, concomitant with an electron transfer back to the heme group. It is important to point out that the redox mechanism obtained in the present study does not require a rotation of the substrate after the N_{60}-O_{57} bond breaking that, according to our simulations, required a significantly higher activation energy. Indeed, a previous study on the Kemp elimination reaction catalysed by the P450-BM3 enzyme showed that, since no base was present in the active site to abstract the proton, an intramolecular proton transfer takes place and, consequently, a rotation of the substrate was necessary to properly align the donor and acceptor atoms.[19] The geometrical analysis of the active site of this aldoxime dehydratase shows that the presence of His320 in the active site and the proper orientation of its imidazole group responsible of the proton transfer in the second step avoids the high energy conformational reorganization detected in the P450-BM3.

On the other side, the presence of a good base in the active site, His320, and the proper pose of the substrate assisted by the heme group, makes available an acid/base mechanism. This mechanism, would require the subtraction of a proton by a base prior to the intramolecular electron transfer that provokes the breaking of the N_{60}-O_{57} bond. The presence of Ser219, acting as an oxyanion hole, together with the full positive electrostatic potential generated by the protein on this key atom, contributes to stabilize the accumulation of negative charge in the oxygen leaving group creating the adequate electrostatic environment. Our previous computational studies[10,11] demonstrated that this effect appears to be crucial to optimize the catalytic power of *de novo* Kemp eliminases designed by Hilvert and co-workers.[9] Obviously, the precise values of the energetics can be tuned if different substrate, with different capabilities to assist the stabilization of the leaving group by charge delocalization were employed.

OxdA promiscuous enzyme, having both a Heme group and a base in the active site, allows exploring whether the preferred mechanism employed by Heme containing enzymes is always a redox mechanism or the alternative acid/base mechanism can be kinetically favoured. Comparison of the results derived from the exploration of both mechanism in OxdA shows how the former renders the most favourable reaction path in a quintet electronic state with a ferromagnetic coupling between the Fe of the Heme group and N atom of the substrate. The obtained activation free energy was 13.6 kcal·mol^{-1}, a value that is very close to the value previously computed for the HG3.17 de novo enzyme (13.8 kcal·mol^{-1}), and it is in agreement with the activation energy that can be deduced from the experimentally measured rate constants by Asano and co-workers at 23 ºC, 16.0 kcal·mol^{-1}.[21] Thus, the results obtained in the present study on OxdA suggest that the enzyme catalyses the reaction through a redox mechanism, despite having a good base properly placed in the active site that could open the possibility of an alternative acid/base mechanism. Anyway, further studies on other Heme containing enzymes must be explored in the future to confirm whether this is a universal conclusion.

Supporting Information

QM/MM optimized structures of the stationary states located along the two reaction mechanisms at the singlet, triplet and quintet electronic states with the Lanl2DZ basis set. QM/MM free energy profiles computed at B3LYP(Lanl2DZ)/MM. Computational details: LRA terms for the reactant states. Time evolution of the QM potential energy of the RC at the singlet, triplet and quintet along the QM/MM MD simulations. NBO analysis of computed on the optimized structures of the stationary states at the three electronic state. Intramolecular proton transfer potential energy surface. This information is available free of charge on the ACS Publications website.

Acknowledgements

This work was supported by Feder funds and the Spanish Ministerio de Ciencia y Universidades (projects PGC2018-094852-B-C21 and PGC2018-094852-B-C22) the Generalitat Valenciana (Grant AICO/2019/195) and Universitat Jaume I (project UJI-B2017-31). Authors acknowledge computational resources from the Servei d'Informàtica of Universitat Jaume I.

References

1 Röthlisberger, D.; Khersonsky, O.; Wollacott, A. M.; Jiang, L.; DeChancie, J.; Betker, J.; Gallaher, J. L.; Althoff, E. A.; Zanghellini, A.; Dym, O.; Albeck, S.; Houk, K. N.; Tawfik, D. S.; Baker, D. Kemp Elimination Catalysts by Computational Enzyme Design. *Nature* **2008**, *453*, 190–195.

2 Casey, M. L.; Kemp, D. S.; Paul, K. G.; Cox, D. D. The Physical Organic Chemistry of Benzisoxazoles. I. The Mechanism of the Base-Catalyzed Decomposition of Benzisoxazoles. *J. Org. Chem.* **1973**, *38*, 2294–2301.

3 Forconi, M. Medium Effects in Biologically Related Catalysis. *Adv. Phys. Org. Chem.* **2015**, *49*, 57–101.

4 Świderek, K.; Tuñón, I.; Moliner, V.; Bertran, J. Computational Strategies for the Design of New Enzymatic Functions. *Arch. Biochem. Biophys.* **2015**, *582*, 68–79.

5 Khersonsky, O.; Röthlisberger, D.; Dym, O.; Albeck, S.; Jackson, C. J.; Baker, D.; Tawfik, D. S. Evolutionary Optimization of Computationally Designed Enzymes: Kemp Eliminases of the Ke07 Series. *J. Mol. Biol.* **2010**, *396*, 1025–1042.

6 Khersonsky, O.; Röthlisberger, D.; Wollacott, A. M.; Murphy, P.; Dym, O.; Albeck, S.; Kiss, G.; Houk, K. N.; Baker, D.; Tawfik, D. S. Optimization of the In-Silico-Designed Kemp Eliminase KE70 by Computational Design and Directed Evolution. *J. Mol. Biol.* **2011**, *407*, 391–412.

7 Khersonsky, O.; Kiss, G.; Röthlisberger, D.; Dym, O.; Albeck, S.; Houk, K. N.; Baker, D.; Tawfik, D. S. Bridging the Gaps in Design Methodologies by Evolutionary Optimization of the Stability and Proficiency of Designed Kemp Eliminase KE59. *Proc. Natl. Acad. Sci. U. S. A.* **2012**, *109*, 10358–10363.

8 Privett, H. K.; Kiss, G.; Lee, T. M.; Blomberg, R.; Chica, R. A.; Thomas, L. M.; Hilvert, D.; Houk, K. N.; Mayo, S. L. Iterative Approach to Computational Enzyme Design. *Proc. Natl. Acad. Sci. U. S. A.* **2012**, *109*, 3790–3795.

9 Blomberg, R.; Kries, H.; Pinkas, D. M.; Mittl, P. R. E.; Grütter, M. G.; Privett, H. K.; Mayo, S. L.; Hilvert, D. Precision Is Essential for Efficient Catalysis in an Evolved Kemp Eliminase. *Nature* **2013**, *503*, 418–421.

10 Świderek, K.; Tuñón, I.; Moliner, V.; Bertran, J. Protein Flexibility and Preorganization in the Design of Enzymes. The Kemp Elimination Catalyzed by HG3.17. *ACS Catal.* **2015**, *5*, 2587–2595.

11 Świderek, K.; Tuñón, I.; Moliner, V.; Bertran, J. Revealing the Origin of the Efficiency of the De Novo Designed Kemp Eliminase HG-3.17 by Comparison with the Former Developed HG-3. *Chem. - A Eur. J.* **2017**, *23*, 7582–7589.

12 Bhowmick, A.; Sharma, S. C.; Head-Gordon, T. The Importance of the Scaffold for de Novo Enzymes: A Case Study with Kemp Eliminase. *J. Am. Chem. Soc.* **2017**, *139*, 5793–5800.

13 Vaissier, V.; Sharma, S. C.; Schaettle, K.; Zhang, T.; Head-Gordon, T. Computational Optimization of Electric Fields for Improving Catalysis of a Designed Kemp Eliminase. *ACS Catal.* **2018**, *8*, 219–227.

14 Welborn, V. V.; Ruiz Pestana, L.; Head-Gordon, T. Computational Optimization of Electric Fields for Better Catalysis Design. *Nat. Catal.* **2018**, *1*, 649–655.

15 Frushicheva, M. P.; Cao, J.; Chu, Z. T.; Warshel, A. Exploring Challenges in Rational Enzyme Design by Simulating the Catalysis in Artificial Kemp Eliminase. *Proc. Natl. Acad. Sci. U. S. A.* **2010**, *107*, 16869–16874.

16 Frushicheva, M. P.; Mills, M. J. L.; Schopf, P.; Singh, M. K.; Prasad, R. B.; Warshel, A. Computer Aided Enzyme Design and Catalytic Concepts. *Curr. Opin. Chem. Biol.* **2014**, *21*, 56–62.

17 Khersonsky, O.; Malitsky, S.; Rogachev, I.; Tawfik, D. S. Role of Chemistry versus Substrate Binding in Recruiting Promiscuous Enzyme Functions. *Biochemistry* **2011**, *50*, 2683–2690.
18 Lamba, V.; Sanchez, E.; Fanning, L. R.; Howe, K.; Alvarez, M. A.; Herschlag, D.; Forconi, M. Kemp Eliminase Activity of Ketosteroid Isomerase. *Biochemistry* **2017**, *56*, 582–591.
19 Li, A.; Wang, B.; Ilie, A.; Dubey, K. D.; Bange, G.; Korendovych, I. V.; Shaik, S.; Reetz, M. T. A Redox-Mediated Kemp Eliminase. *Nat. Commun.* **2017**, *8*, 14876-14883.
20 Reetz, M. T. Directed Evolution of Artificial Metalloenzymes: A Universal Means to Tune the Selectivity of Transition Metal Catalysts? *Acc. Chem. Res.* **2019**, *52*, 336–344.
21 Miao, Y.; Metzner, R.; Asano, Y. Kemp Elimination Catalyzed by Naturally Occurring Aldoxime Dehydratases. *ChemBioChem* **2017**, *18*, 451–454.
22 Pan, X. L.; Cui, F. C.; Liu, W.; Liu, J. Y. QM/MM Study on the Catalytic Mechanism of Heme-Containing Aliphatic Aldoxime Dehydratase. *J. Phys. Chem. B* **2012**, *116*, 5689–5693.
23 Liao, R. Z.; Thiel, W. Why Is the Oxidation State of Iron Crucial for the Activity of Heme-Dependent Aldoxime Dehydratase? A QM/MM Study. *J. Phys. Chem. B* **2012**, *116*, 9396–9408.
24 Nomura, J.; Hashimoto, H.; Ohta, T.; Hashimoto, Y.; Wada, K.; Naruta, Y.; Oinuma, K. I.; Kobayashi, M. Crystal Structure of Aldoxime Dehydratase and Its Catalytic Mechanism Involved in Carbon-Nitrogen Triple-Bond Synthesis. *Proc. Natl. Acad. Sci. U. S. A.* **2013**, *110*, 2810–2815.
25 Søndergaard, C. R.; Olsson, M. H. M.; Rostkowski, M.; Jensen, J. H. Improved Treatment of Ligands and Coupling Effects in Empirical Calculation and Rationalization of p K a Values. *J. Chem. Theory Comput.* **2011**, *7*, 2284–2295.
26 Olsson, M. H. M.; SØndergaard, C. R.; Rostkowski, M.; Jensen, J. H. PROPKA3: Consistent Treatment of Internal and Surface Residues in Empirical p K a Predictions. *J. Chem. Theory Comput.* **2011**, *7*, 525–537.
27 Phillips, J. C.; Braun, R.; Wang, W.; Gumbart, J.; Tajkhorshid, E.; Villa, E.; Chipot, C.; Skeel, R. D.; Kalé, L.; Schulten, K. Scalable Molecular Dynamics with NAMD. *J. Comput. Chem.* **2005**, *26*, 1781–1802.
28 MacKerell, A. D.; Bashford, D.; Bellott, M.; Dunbrack, R. L.; Evanseck, J. D.; Field, M. J.; Fischer, S.; Gao, J.; Guo, H.; Ha, S.; Joseph-McCarthy, D.; Kuchnir, L.; Kuczera, K.; Lau, F. T. K.; Mattos, C.; Michnick, S.; Ngo, T.; Nguyen, D. T.; Prodhom, B.; Reiher, W. E.; Roux, B.; Schlenkrich, M.; Smith, J. C.; Stote, R.; Straub, J.; Watanabe, M.; Wiórkiewicz-Kuczera, J.; Yin, D.; Karplus, M. All-Atom Empirical Potential for Molecular Modeling and Dynamics Studies of Proteins †. *J. Phys. Chem. B* **1998**, *102*, 3586–3616.
29 Vanommeslaeghe, K.; Hatcher, E.; Acharya, C.; Kundu, S.; Zhong, S.; Shim, J.; Darian, E.; Guvench, O.; Lopes, P.; Vorobyov, I.; Mackerell, A. D. CHARMM General Force Field: A Force Field for Drug-like Molecules Compatible with the CHARMM All-Atom Additive Biological Force Fields. *J. Comput. Chem.* **2010**, *31*, 671–690.
30 Mackerell, A. D.; Feig, M.; Brooks, C. L. Extending the Treatment of Backbone Energetics in Protein Force Fields: Limitations of Gas-Phase Quantum Mechanics in Reproducing Protein Conformational Distributions in Molecular Dynamics Simulation. *J. Comput. Chem.* **2004**, *25*, 1400–1415.
31 Trott, O.; Olson, A. J. AutoDock Vina: Improving the Speed and Accuracy of Docking with a New Scoring Function, Efficient Optimization, and Multithreading. *J. Comput. Chem.* **2009**, *31*, 455-461.
32 Bitzek, E.; Koskinen, P.; Gähler, F.; Moseler, M.; Gumbsch, P. Structural Relaxation Made Simple. *Phys. Rev. Lett.* **2006**, *97*, 170201–170204.
33 Guénolé, J.; Nöhring, W. G.; Vaid, A.; Houllé, F.; Xie, Z.; Prakash, A.; Bitzek, E. Assessment and Optimization of the Fast Inertial Relaxation Engine (Fire) for Energy Minimization in Atomistic Simulations and Its Implementation in Lammps. *Comput. Mater. Sci.* **2020**, *175*, 109584–109593.

34 Darden, T.; York, D.; Pedersen, L. Particle Mesh Ewald: An N·log(N) Method for Ewald Sums in Large Systems. *J. Chem. Phys.* **1993**, *98*, 10089–10092.
35 Lee, C.; Yang, W.; Parr, R. G. Development of the Colle-Salvetti Correlation-Energy Formula into a Functional of the Electron Density. *Phys. Rev. B* **1988**, *37*, 785–789.
36 Becke, A. D. Density-Functional Thermochemistry. III. The Role of Exact Exchange. *J. Chem. Phys.* **1993**, *98*, 5648–5652.
37 Hay, P. J.; Wadt, W. R. Ab Initio Effective Core Potentials for Molecular Calculations. Potentials for K to Au Including the Outermost Core Orbitale. *J. Chem. Phys.* **1985**, *82*, 299–310.
38 Frisch, M. J.; Trucks, G. W.; Schlegel, H. B.; Scuseria, G. E.; Robb, M. A.; Cheeseman, J. R.; Scalmani, G.; Barone, V.; Mennucci, B.; Petersson, G. A.; Nakatsuji, H.; Caricato, M.; Li, X.; Hratchian, H. P.; Izmaylov, A. F.; Bloino, J.; Zheng, G.; Sonnenberg, J. L.; Hada, M.; Ehara, M.; Toyota, K.; Fukuda, R.; Hasegawa, J.; Ishida, M.; Nakajima, T.; Honda, Y.; Kitao, O.; Nakai, H.; Vreven, T.; Montgomery, J. A., Jr.; Peralta, J. E.; Ogliaro, F.; Bearpark, M.; Heyd, J. J.; Brothers, E.; Kudin, K. N.; Staroverov, V. N.; Kobayashi, R.; Normand, J.; Raghavachari, K.; Rendell, A.; Burant, J. C.; Iyengar, S. S.; Tomasi, J.; Cossi, M.; Rega, N.; Millam, J. M.; Klene, M.; Knox, J. E.; Cross, J. B.; Bakken, V.; Adamo, C.; Jaramillo, J.; Gomperts, R.; Stratmann, R. E.; Yazyev, O.; Austin, A. J.; Cammi, R.; Pomelli, C.; Ochterski, J. W.; Martin, R. L.; Morokuma, K.; Zakrzewski, V. G.; Voth, G. A.; Salvador, P.; Dannenberg, J. J.; Dapprich, S.; Daniels, A. D.; Farkas, O.; Foresman, J. B.; Ortiz, J. V.; Cioslowski, J.; Fox, D. J. Gaussian 09, Revision E.01; Gaussian, Inc.: Wallingford, CT, 2009.
39 Weigend, F.; Ahlrichs, R. Balanced basis sets of split valence, triple zeta valence and quadruple zeta valence quality for H to Rn: Design and assessment of accuracy. *Phys. Chem. Chem. Phys.* **2005**, *7*, 3297–305.
40 Grimme, S.; Ehrlich, S.; Goerigk, L. Effect of the Damping Function in Dispersion Corrected Density Functional Theory. *J. Comput. Chem.* **2011**, *32*, 1456–1465.
41 Grimme, S.; Antony, J.; Ehrlich, S.; Krieg, H. A Consistent and Accurate Ab Initio Parametrization of Density Functional Dispersion Correction (DFT-D) for the 94 Elements H-Pu. *J. Chem. Phys.* **2010**, *132*, 154104–154122.
42 Glendening, E.D; Reed, A.E.; Carpenter, J.E.; Weinhold, F. NBO, Version 3.1
43 Martí, S.; Moliner, V.; Tuñón, I. Improving the QM/MM Description of Chemical Processes: A Dual Level Strategy to Explore the Potential Energy Surface in Very Large Systems. *J. Chem. Theory Comput.* **2005**, *1*, 1008–1016.
44 Hummer, G.; Szabo, A. Calculation of Free-Energy Differences from Computer Simulations of Initial and Final States. *J. Chem. Phys.* **1996**, *105*, 2004–2010.
45 Chipot, C. Free Energy Calculations in Biological Systems. How Useful Are They in Practice? *Lecture Notes in Computational Science and Engineering*, Springer-Verlag: Berlin Heidelberg, 2006; Vol. 49, pp 185–211.

Table of Contents Graphic